Structural and functional characterizations reveal the importance of a zinc binding domain in Bloom's syndrome helicase

Rong-bin Guo, Pascal Rigolet, Loussiné Zargarian, Serge Fermandjian and Xu Guang Xi*

Laboratoire de Biotechnologies et Pharmacologie Génétique Appliquée CNRS UMR 8113, Ecole Normale Supérieure (ENS) Cachan, 61 avenue du Président Wilson, 94235 Cachan cedex, France

ABSTRACT

Bloom's syndrome (BS) is an autosomal recessive human disorder characterized by genomic instability and a predisposition to a wide variety of cancers. The gene mutated in BS, *BLM*, encodes a protein containing three domains: an N-terminal domain whose function remains elusive, a helicase domain characterized by seven 'signature' motifs conserved in a wide range of helicases and a C-terminal extension that can be further divided into two sub-domains: RecQ-Ct and HRDC. The RecQ-Ct domain appears essential because two point-mutations altering highly conserved cysteine residues within this domain have been found in BS patients. We report herein that BLM contains a zinc ion. Modelling studies suggest that four conserved cysteine residues within the RecQ-Ct domain coordinate this zinc ion and subsequent mutagenesis studies further confirm this prediction. Biochemical and biophysical studies show that the ATPase, helicase and DNA binding activities of the mutants are severely modified. Structural analysis of both wild-type and mutant proteins reveal that alteration of cysteine residues does not significantly change the overall conformation. The observed defects in ATPase and helicase activities were inferred to result from a compromise of DNA binding. Our results implicate an important role of this zinc binding domain in both DNA binding and protein conformation. They could be pivotal for understanding the molecular basis of BS disease.

INTRODUCTION

Bloom's syndrome (BS) is a rare, autosomal recessive disease that results from the mutational inactivation of the human RecQ family helicase encoded by the *BLM* gene chromosome 15 (1). Individuals afflicted with BS display a pleiotropic array of syndromes, features associated with pre- and postnatal growth retardation, sunlight sensitivity, subfertility in females and infertility in males, immunodeficiency, and a marked predisposition to a variety of cancers, including solid tumours and leukaemia. Cells from BS patients exhibit a strikingly high level of chromosomal instability, including chromosome breakage, translocation, increased rates of sister-chromatid exchange (SCE) and telomeric association (2–4).

The gene defective in BS encodes the Bloom syndrome protein (BLM) which consists of 1417 amino acids. It belongs to the RecQ DNA helicase family. Biochemical analysis shows that BLM is a DNA-dependent ATPase and ATP-dependent DNA helicase that displays a 3′–5′ polarity (5). DNA helicases are a class of enzymes implicated in all aspects of DNA metabolism processes including DNA replication, repair, transcription and recombination (6). Consistent with its helicase function, BLM localizes to some sites of ongoing DNA replication, particularly during the late S phase or following replication arrest (7). BLM not only unwinds the canonical Watson–Crick duplex, but also recognizes and disrupts alternative DNA structures such as the Holliday junction, the triple helix and the highly stable G-quadruplex structure (8–13). Besides its helicase domain, BLM contains two conserved domains in its C-terminal region, namely the HRDC (Helicase, RNase D Conserved) and RecQ-Ct domains. The HRDC domain which is distal to the C-terminus may modulate the helicase function via auxiliary contacts to DNA (14). The RecQ-Ct (RecQ C-terminal) domain located just after the conserved seven signature motifs is unique to the RecQ family of helicases. Although the C-terminal region is devoid of catalytic activity, it is essential for the maintenance of chromosomal stability and nucleolar localization in human cells (15). It is well documented that the BLM helicase performs its diverse functions through protein–protein interactions with a variety of nuclear proteins involved in various aspects of the DNA metabolism such as BRCA1, ATM,

*To whom correspondence should be addressed. Tel: +33 1 47 40 68 92; Fax: +33 1 47 40 76 71; Email: xi@lbpa.ens-cachan.fr

MLH1, MSH2, MSH6, Rad51, topoisomerase IIIα, replication protein A, FEN-1 and replication factor C (16–20). Among these, MLH1, topoisomerase IIIα, Rad51 and FEN-1 interact with the C-terminal region of BLM. Remarkably, FEN-1 activity is dramatically stimulated by the BLM C-terminal region containing the RecQ-Ct domain (21).

In this work, we are interested specifically in the function of the RecQ-Ct domain due to three independent observations. First, a sequence homology analysis among the known members of the RecQ helicase family has identified a putative zinc binding domain in the RecQ-Ct domain of BLM (22). Consistent with this prediction, 3D structure analyses have revealed the existence of a zinc binding domain in the RecQ-Ct domain of *Escherichia coli* RecQ helicase that is conserved by sequence homology in BLM (23). Second, two disease-causing BLM missense mutations map to Cys-1036 and Cys-1055 (24). These residues are broadly conserved in the RecQ-Ct region of the RecQ helicase family and are possibly implicated in the zinc binding domain formation. Third, our previous studies have shown that the zinc binding domain of *E.coli* RecQ helicase plays a crucial role in both DNA binding and protein folding (25). These observations stimulated us to determine whether the BLM also harbours a functional zinc binding domain and then to study, in greater detail, the relationships between the structure and the function of the zinc binding domain.

Here, we report the biochemical and biophysical characterization of the helicase core containing the RecQ-Ct domain of BLM and that of several mutant derivatives carrying alterations in the four conserved cysteine positions of the zinc binding motif. We have found that BLM bears a zinc binding domain that is important for DNA binding, ATPase and helicase activities. Our study provides strong evidence for the molecular basis of certain missense mutations that cause BS, gaining insight into both the function of BLM and the molecular basis of BS pathogenicity.

MATERIALS AND METHODS

Materials

4-(2-Pyridylazo) resorcinol disodium salt (PAR), EDTA, DTT, 2-mercaptoethanol, ATP, 5,5′-dithiobis-(2-nitrobenzoic acid) (DTNB) and trypsin were obtained from Sigma. [α-^{32}P]ATP was obtained from Amersham Bioscience. Chelex$^®$ 100 resin was purchased from Bio-Rad. The *N*-methylanthraniloyl derivatives of adenine nucleotides were synthesized according to Hiratsuka (26), and purified on DEAE-cellulose using a gradient of triethylammonium bicarbonate.

Methods

Sequences alignment and theoretical modelling. Comparative sequence analysis between the helicase core of BLM and *E.coli* RecQ was performed with ClustalW (27) and followed by manual adjustment. For the zinc binding domain region, where insertions occur, we decided to refer to the multiple alignments shown in Figure 2A, involving eight known helicases of the RecQ family.

Based on this alignment, we have folded the amino acid sequence of the helicase core of BLM onto the template crystal structure of the apo *E.coli* RecQ (23) by homology modelling using MODELLER software (28). The score of 35% identity between the two sequences was sufficiently high to obtain a realistic model for BLM helicase core. The Zn^{2+} ion has been included in the modelling schedule. The model has been refined using the optimize routine of Modeler including molecular dynamic refinement steps, temperature ranging from 200 to 1000 K. Energy was finally minimized by the conjugate gradients optimization method. In the *E.coli* RecQ, the cysteine residue in the C2 position is sterically restrained between a proline, one residue before, and a glycine, one residue after the cysteine. During the refinement process, it became possible that the cysteine C2 in BLM model could be included in a small α-helix ended by a proline residue. This model was easier to refine than models with a loop in this region. The credibility of this secondary structure element is reinforced by the presence of two proline residues in good positions to delimit the α-helix. The stereochemistry of the final model has been checked with PROCHECK, and its fold has been evaluated using the protein structure MultiEvaluation tool invoking EVAL123D (29), Verif3D (30) and Prosa II (31). Packing quality of the homology model was also investigated by the calculation of WHATIF Quality Control Value (32). The results confirmed that a reasonable model was obtained. Figure 2B–D were generated with MOLSCRIPT and rendered with Raster3D. Figure 2E and F have been drawn with GRASP software (33).

Recombinant proteins. Previous studies have shown that the RecQ core of BLM consisting of the DEAH, RecQ-Ct and HRDC domains displays similar enzymatic properties as the full-size BLM (34). Therefore, the truncated BLM protein containing residues 642–1290 (BLM$^{642–1290}$) and their different modified forms were used in this study. A plasmid for expression of a truncated form of the helicase core consisting of the DEAH containing domain, the RecQ-Ct and HRDC domains (amino acid residues 642–1290) was generated by inserting the truncated *BLM* gene between the NdeI and XhoI cloning sites of the pET15b expression plasmid (Novagen). In this context, BLM is fused in frame with an N-terminal peptide containing six tandem histidine residues, and expression of the His-tagged protein is driven by a T7 RNA polymerase promoter. The resulting recombinant plasmid, pET-BLM$^{642–1290}$, was transformed into *E.coli* BL21-Codon-Plus (Stratagene). One litre culture of *E.coli* BL21-CodonPlus/ pET-BLM$^{642–1290}$ was grown at 37°C in Luria–Bertani medium containing 50 μg/ml ampicillin and 30 μg/ml chloramphenicol until the A_{600} reached 0.5. The culture was adjusted to 0.4 mM isopropyl-β-D-thiogalactopyranoside, and the incubation was continued at 18°C for 20 h. The cells were then harvested by centrifugation, and the pellet was stored at −80°C. All subsequent procedures were performed at 4°C. Thawed bacteria pellets were resuspended in 5 ml of lysis buffer A [20 mM Tris–HCl, pH 7.9, 500 mM NaCl, 10% glycerol, 0.1% Triton X-100 and 1 mM phenylmethylsulfonyl fluoride (PMSF)], and cell lysis was achieved by a French pressure cell. The lysates were sonicated to reduce viscosity, and any insoluble material was removed by centrifugation at 13 000 r.p.m. with a GA20 rotor from Beckman for 45 min. The soluble extract was applied to a 20 ml column of nickel-nitrilotriacetic acid–agarose (Qiagen) that had been equilibrated with buffer A. The column was washed with the same buffer and then eluted stepwise with buffer A containing 50,

100, 200, 500 and 1000 mM imidazole. The recombinant BLM protein was retained on the column and recovered in the 200 mM imidazole eluate. This fraction was further purified by FPLC size exclusion chromatography (Superdex 200; Amersham Bioscience). Following dialysis against buffer B (20 mM Tris–HCl, pH 7.9, 150 mM NaCl and 10% glycerol), BLM was stored at −80°C. The protein concentration was determined by the Bio-Rad dye method with BSA as the standard.

Site-directed mutagenesis, expression and purification of mutant proteins. The pET-BLM$^{642-1290}$ construct encompassing amino acids 642 (nt 1920) to 1290 (nt 3870) was used as the target plasmid for site-directed mutagenesis. All point mutations were constructed using recombinant PCR, with the desired mutations introduced in the internal mutagenic primers (Table 1). To ensure that only the desired mutation was introduced, the PCR portions were sequenced with the dideoxy DNA sequencing method. The procedure of the expression and purification of the mutant BLMs is essentially the same as wild-type protein with the exception that the lysis buffer A used for mutant proteins contains leupeptin and pepstatin at 5 µg/ml, respectively. The purity of the BLM and the mutant proteins were determined by SDS–PAGE analysis and were found to be >98% (Figure 1).

DNA substrates preparation. PAGE purified oligonucleotides listed in Table 1 were purchased from Proligo (France). The 5′ and 3′ single-stranded DNA (ssDNA) tails of 23mer duplexed substrates were formed by annealing oligonucleotides A and B, and used for both DNA binding and helicase unwinding experiments. The duplex DNA substrates were prepared as described previously (35) with the exception that oligonucleotides used for fluorescence assays were not 5′-^{32}P-end-labelled. G4 DNA was prepared and isolated as described (9). Briefly, 250 µM DNA substrates F21 were denatured in 1× TE containing 1 M

NaCl or 1 M KCl by heating at 95°C for 10 min. The denatured DNA was then annealed at 37°C for 48 h. The annealed products were separated on 8% native PAGE containing 10 mM KCl at 4°C for 12 h with constant current of 20 mA. Bands corresponding to tetrameric G-quadruplex, dimeric G-quadruplex and monomeric oligonucleotide were identified according to their relative mobility by UV-shadowing or autoradiography. The identified bands were then excised from the gel and eluted with TE (pH 8.0) containing 50 mM NaCl and 20 mM KCl. The purified G-quadruplex DNA was precipitated with ethanol and stored in 10 mM Tris–HCl (pH 7.5).

Quantification of Zn^{2+} bound to BLM and mutant BLM helicases. The Zn^{2+} content of BLM$^{642-1290}$ and of mutant
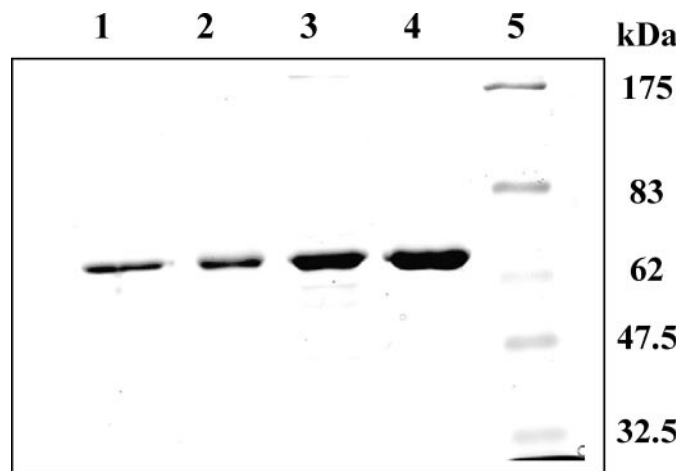
Figure 1. Analysis of the purified BLM and mutant proteins by SDS PAGE. The proteins were resolved in 10% SDS–polyacrylamide gel and stained with Coomassie blue: lane 1, C1055N/C1063N (5 µg); lane 2, C1063N (5 µg); lane 3, C1050N (10 µg); and lane 4, BLM$^{642-12090}$ (10 µg). The positions of marker proteins (in kDa) are indicated at the right.

Table 1. Sequence of oligonucleotides used for site-directed mutagenesis and DNA substrate

BLM	Protein sequences	Recombinant or mutagenic PCR primer (5′–3′)
WT	CR*Xn*C*Xn*CDXC	F-GGAATTCATATGGAGCGTTTCCAAAGTCTTAGTTTTCCT
		R-CCGCTCGAGTTACGATGTCCATTCAGAGTATTTCTGTAA
C1036F	**F**R*Xn*C*Xn*CDXC	F-GAAAATATAACGG**AATTC**AGGAGAATACAGCTT
		R-AAGCTGTATTCTCCTGAATTCCGTTATATTTTC
C1036N	**D**R*Xn*C*Xn*CDXC	F-GAAAATATAACGGA**AAAC**AGGAGAATACAGCTT
		R-AAGCTGTATTCTCCTGTTTTCCGTTATATTTTC
C1055N	CR*Xn***N***Xn*CDXC	F-TTTAATCCTGATTTTA**ATAAG**AAACACCCAGAT
		R-ATCTGGGTGTTTCTTATTAAAATCAGGATTAAA
C1055S	CR*Xn***S***Xn*CDXC	F-AATCCTGATTTTT**CTAAG**AAACACCCA
		R-TGGGTGTTTCTTAGAAAAATCAGGATT
C1063N	CR*Xn*C*Xn***N**DXC	F-CACCCAGATGTTTCT**AATGAT**AATTGCTGT
		R-ACAGCAATTATCATTAGAAACATCTGGGTG
C1055N/C1063N	CR*Xn***N***Xn***N**DXC	F-CACCCAGATGTTTCT**AATGAT**AATGACTGT
		R-ACAGTCATTATCATTAGAAACATCTGGGTG
R1037A	C**A***Xn*C*Xn*CDXC	F-AATATAACGGAATGC**GC**GAGAATACAGCTT
		R-AAGCTGTATTCTC**GC**GCATTCCGTTATATT
D1064A	CR*Xn*C*Xn*C**A**XC	F-GATGTTTCTTGT**GCT**AATTGCTGTTGT
		R-ACAACAGCAATT**AGC**ACAAGAAACATC

DNA substrate	Length	DNA substrate sequences
A	44	GCACTGGCCGTCGTTTTACGGTCGTGACTGGGAAAACCCTGGCG
B	45	TTTTTTTTTTTTTTTTTTTTTTTTAGCCGTAAAACGACGGCCAGTGC
F21	21	Fluo-GGGTTAGGGTTAGGGTTAGGG

Bold format represents the mutated residues

helicases was measured using PAR, a reporter dye that absorbs light at 490 nm when bound to Zn^{2+} (36). In order to more precisely quantify the zinc content of both wild-type ($BLM^{642-1290}$) and BLM mutant helicases, all buffers were treated with Chelex® 100 resin. The enzymes were dialysed against the EDTA-free Chelex®-treated buffer, passed over a 10 cm column of Chelex®-100 and re-concentrated. To facilitate zinc release, enzymes (~1 nmol in a volume of 40 µl) were first denatured with Chelex®-treated 7 M guanidine HCl, and then transferred to a 1 ml cuvette. PAR was added into the cuvette for a final concentration of 100 µM and the volume adjusted to 1 ml with buffer B (20 mM Tris–HCl pH 8.0 and 150 mM NaCl). The absorbance was recorded from 350 to 600 nm on a UVIKON spectrophotometer 941 (Kontron) at 25°C. The quantity of zinc ion was determined using the absorbance coefficient for the $(PAR)_2 \cdot Zn^{+2}$ complex ($\varepsilon_{500} = 6.6 \times 10^4 \ M^{-1} \ cm^{-1}$). As a control, a solution of 20 µM pure $ZnCl_2$ was quantified in the same condition of the samples.

Quantitation of free thiol groups in BLM. Both untreated and Zn^{2+}-extracted BLM proteins were subjected to DTNB titrations under native conditions. The enzyme samples were fresh preparations that had been isolated using buffers to which no reductant had been added. Any thiol-bearing component of the cell extracts (either small or macro-molecules) should have been removed by the chromatography over Ni-NTA and the exchange (by size-exclusion chromatography or dialysis) of BLM-bearing column fractions into 20 mM Tris–HCl buffer, pH 7.9, containing $MgCl_2$ (5 mM), KCl (250 mM), 10% glycerol and EDTA (0.1 mM). The protein concentration ranging from 4.5 to 15.2 µM, DTNB (20 eq. relative to BLM) was added as a solution (10 mM) in the same buffer. Control incubations were prepared by adding the same amount of DTNB to the same buffer (with no protein). The final mixtures (400 µl) were incubated 20–30 min at room temperature, and the intensely yellow dianion of 5-thio-2-nitrobenzoic acid was quantified by subtracting the $A_{412 \ nm}$ of the control incubation from the $A_{412 \ nm}$ of each sample and using an extinction coefficient of 14 150 $M^{-1} cm^{-1}$ (37). These values were converted to [thiolsfree]. All titrations were performed in duplicate.

Circular dichroism spectroscopy measurements. Circular dichroism (CD) spectra were recorded on a Jobin-Yvon Marker IV high sensitivity dichrography linked to a PC micro-processor. The samples were extensively dialysed against buffer C (50 mM Tris–HCl, pH 8.9 and 50 mM NaCl) and were analysed in quartz cells with path lengths of 1 mm. All spectra were recorded with a 1 nm step, were signal-averaged over at least four scans and were base-line corrected by substracting a buffer spectrum. The results were expressed as mean residue ellipticity (MRE) in deg cm^2 dmol^{-1} defined as

$$MRE = \theta_{obs}(m \deg)/10 \times n \times Cp \times l$$

where θ_{obs} is the CD in millidegree; n, the number of amino acid residues; l, the pathlength of the cell in centimetres; and Cp, the molar fraction. The relative content in α-helix was deduced according to Zhong and Johnson (38): % α-helix = $\Delta\varepsilon_{222 \ nm} \times (-10)$, where $\Delta\varepsilon_{222 \ nm}$ is the CD per residue at 222 nm and is related to $[\theta]_{222}$ by $\Delta\varepsilon_{222 \ nm} = [\theta]_{222}/3300$. A protein concentration of 0.15 mg/ml was used for far-UV CD measurements.

Size exclusion chromatography. Size exclusion chromatography was performed at 18°C using an FPLC system (AKTA, Amersham Bioscience) on a Superdex 200 (analytical grade) column equilibrated with elution buffer. Fractions of 0.5 ml were collected at a flow rate of 0.4 ml/min, and absorbance was measured at 280 and 260 nm. The R_s values (R_s designates the Stoke radius of the protein) of wild-type and mutant BLMs were determined from the plot of log R_s versus K_{av} using the different Stokes radii of the standards. The partition coefficient K_{av} was calculated using the formula $K_{av} = (V_e - V_0)/(V_t - V_0)$, where V_e is the elution volume of the sample, V_0 is the excluded volume of the column, V_t is the total volume of the column. The excluded volume, V_0 (7.52 ml) and the total volume, V_t (23.5 ml) were measured by calibration with Dextran blue and thymidine. The calibration graph of log R_s versus K_{av} was constructed using a high and low molecular weight calibration kit from Sigma: cytochrome c (Mw = 12.4 kDa; R_s = 12 Å), carbonic anhydrase (Mw = 29 kDa; R_s = 22.5 Å), albumin (Mw = 67 kDa; R_s = 35.5 Å), phosphorylase b (Mw = 97.4 kDa; R_s = 38.75 Å), thyroglobulin (Mw = 669 kDa; R_s = 85 Å). Assuming similar shape factors, the plot calibration of log Mw versus K_{av} allowed the determination in first approximation of the molecular weight of the enzyme. Gel filtration chromatography was performed using a standard elution buffer (50 mM Tris–HCl, pH 7.5, 300 mM NaCl and 0.1 mM EDTA) with 1 mM ATP and 1 mM Mg(OAc)$_2$. BLM proteins (5 µM) were incubated in the elution buffer with ATP and $MgCl_2$ for 2 min prior to injection onto the column.

Protein–DNA binding assay

Electrophoretic mobility shift assay. Protein at concentrations ranging from 2.5 to 2000 nM was incubated with 2.5 nM 23mer duplexed oligonucleotide labelled at the 5′ end using [γ-^{32}P]ATP and T4 polynucleotide kinase. Incubations were carried out at room temperature for 20 min in DNA binding buffer [50 mM Tris–HCl, pH 7.5, 1 mM DTT, 50 mM NaCl and 10% (v/v) glycerol]. Samples were subsequently subjected to electrophoresis through a non-denaturing 15% polyacrylamide gel [acrylamide to bis-acrylamide, 37.5:1 (w/w)] run in TBE buffer at 100 V to separate protein–DNA complex from free DNA. Gels were dried and visualized by autoradiography.

Fluorescence polarization assay. Binding of $BLM^{642-1290}$ and its different mutant proteins to DNA was analysed by fluorescence polarization using a Beacon fluorescence polarization spectrophotometer (PanVera). A 23mer duplexed oligonucleotide labelled with fluorescein on the 5′ end of one strand was used in this study. Varying amounts of proteins were added to a 150 µl aliquot of binding buffer (25 mM Tris–HCl, pH 8, 30 mM sodium chloride, 3 mM magnesium acetate and 0.1 mM DTT) containing 2 nM of the fluorescein-labelled DNA. Each sample was allowed to equilibrate in solution for 5 min, after which fluorescence polarization was measured. A second reading was taken after 10 min, in order to ensure that the mixture had equilibrated. Less than 5% change was observed between the 5 min measurement and the 10 min measurement indicating that equilibrium was reached. The equilibrium dissociation constant was determined by plotting polarization as a function of protein concentration and fitting the data to the Michaelis–Menten or Hill equation by using the program KaleidaGraph (Synergy Software).

ATPase assay. The ATPase activity was determined by a measure of the radioactive γ-^{32}Pi liberated during hydrolysis (39). Briefly, the measurement was carried out at 25 or 37°C in a reaction mixture containing 1.5 μM (nt) heat-denatured HindIII-cut pGEM-7Zf linear DNA at the indicated concentration of ATP. The reactions were initiated by the addition of BLM helicase into a 100 μl reaction mixture and stopped by pipetting 80 μl aliquots from the reaction mixture every 30 s into a hydrochloric solution of ammonium molybdate. The liberated radioactive γ-^{32}Pi was extracted with a solution of 2-butanol ($C_4H_{10}O$)/benzene (C_6H_6)/acetone (C_3H_6O)/ammonium molybdate [$(NH4)_6Mo_7O_{24}$, 150 μM] (750:750:15:1) saturated with water. An aliquot of the organic phase was counted in 6 ml of Aquasol.

ATP binding assays. The UV cross-linking assay was first used to assess the ATP binding ability of both wild-type and mutant BLM proteins (40). One microgram of wild-type or mutant helicase proteins were premixed in 10 μl of a buffer containing 20 mM HEPES–KOH, pH 7.5 and 5 mM Mg(CH_3CO_2)$_2$. Then 2.5 μCi (2 pmol) of [γ-^{32}P]ATP (3000 Ci/mmol; Amersham) and 150 pmol of cold ATP were added. The reaction mixture was incubated on ice for 15 min and was then irradiated using a UV cross-linker (Stratagene) (254 nm) situated at a distance of 4 cm for 5 min. Samples were boiled in sample buffer (100 mM Tris–HCl, pH 6.8, 2% SDS, 20% β-mercaptoethanol, 20% glycerol, 4 mM EDTA and 0.01% bromophenol blue) for 5 min and were then separated by SDS–12.5% PAGE. The gels were stained with Coomassie brilliant blue, dried and processed for autoradiography.

Fluorescence measurements. The above UV cross-linking assay is a non-equilibrium method of measuring ATP binding and cannot be used to determine the apparent dissociation value. We therefore used a fluorescent nucleotide analogue (mantATP) to determine the apparent dissociation values between the wild type and mutants. Fluorescence spectra were measured using a PiStar-180 spectrometer (Applied Photophysics) or a Fluoro Max-2 spectrofluorimeter (Jobin Yvon, Spex Instruments S.A., Inc.) at 25°C. In a 10 × 10 × 40 quartz cuvette, 0.5 μM protein in 1 ml reaction buffer was excited at 280 nm and fluorescence emission was monitored at 350 nm. MantATP binding to protein was measured by exciting BLM proteins at 280 nm and measuring the fluorescence of mantATP at 440 nm due to FRET. Both sample dilution and inner filter effects were taken into account and the observed fluorescence intensity was corrected (41).

The apparent K_d values were determined by fitting the fluorescence intensity values to the following equation:

$$F = F_s + f_d x + f_c \frac{(x + 0.5 + K_d) - \sqrt{(x + 0.5 + K_d)^2 - 2x}}{2},$$

1

where F_s is the starting fluorescence of the reaction mixture; f_d, the fluorescence coefficient of free mantATP; f_c, the fluorescence coefficient of complex formed; x, the total concentration of mantATP and K_d, the apparent constant dissociation.

Helicase assay
Radiometric helicase assay. DNA helicase activity was measured in reaction mixtures (15 μl) containing 25 mM HEPES–NaOH, pH 7.5, 25 mM CH_3CO_2Na, 7.5 mM (CH_3CO_2)$_2$Mg, 2 mM ATP, 1 mM DTT, 0.1 mg/ml BSA, the indicated ^{32}P-labelled partial duplex DNA substrate (10 fmol, 3000 c.p.m./fmol) and enzyme fraction. After incubation at 37°C for 20 min, 4 μl of 5× loading buffer (50 mM EDTA, 0.5% SDS, 0.1% xylene cyanol, 0.1% bromophenol blue and 50% glycerol) was added, and aliquots were loaded onto a 12% polyacrylamide gel containing 0.1% SDS in 1× TBE (90 mM Tris, 90 mM boric acid and 1 mM EDTA, pH 8.3) and electrophoresed for 1.5 h at 150 V.

Fluorometric helicase kinetic assay. An unwinding assay was performed using a Beacon 2000 polarization instrument, according to Xu *et al.* (42). An appropriate quantity of fluorescein-labelled duplex oligonucleotide was added to the helicase unwinding buffer (150 μl total) in a temperature-controlled cuvette. The anisotropy was measured successively until it stabilized. The helicases were then added into the reaction tube. When the higher anisotropy value became stable, the unwinding reaction was initiated by the rapid addition of ATP solution to give a final concentration of 1 mM. The decrease of the anisotropy was recorded every 8 s until it became stable. The unwinding buffer contained 25 mM Tris–HCl (pH 8.0), 30 mM NaCl, 3 mM (CH_3CO_2)$_2$Mg and 0.1 mM DTT.

RESULTS

We used a wide array of biochemical and biophysical methods, including structural modelling and site-directed mutagenesis, to better understand and define the function of the zinc binding domain in the BS protein. Conventional gel-based assays allowed to qualitatively assess the helicase and DNA binding activities. The related parameters were further determined quantitatively by fluorometric measurements. The combination of these approaches enabled us to analyse the role of the zinc binding domain in precise detail.

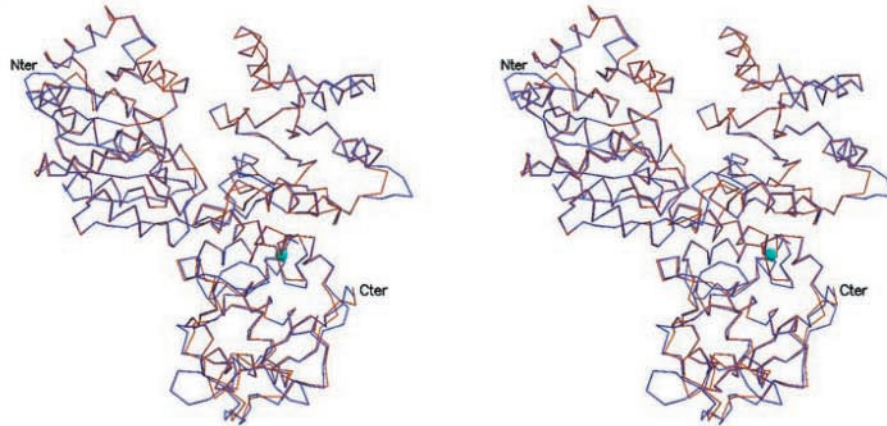### Homology modelling predicts a zinc binding domain in BLM

The final alignment of the sequences of the helicase core from BLM and from *E.coli* RecQ helicase showed that 35% of the residues are identical and 20% highly similar. In the zinc binding domain region, we took into account 8 RecQ sequences (Figure 2A) with all the residues known to be conserved through evolution (25) perfectly aligned. The score of sequence identity between the BLM and *E.coli* RecQ sequences, largely above the well-established limit of 30% (28), allowed us to obtain a realistic model for the 3D structure of the BLM helicase core (Figure 2B) starting from the crystal structure of *E.coli* RecQ helicase as a template. Since the template structure does not contain the HRDC domain, we only modelled the BLM helicase core Phe-644 to Ser-1195 of the enzyme tested for function (residues 642–1290). Thus, our model does not include the HRDC domain present in the BLM construct used in biochemical studies. The stereochemistry, energy and packing quality tests applied confirmed that a reasonable model was obtained, suitable to investigate the zinc binding motif and to explore the role of different conserved residues.

The modelled BLM helicase core comprises 36 residues more than the catalytic core of *E.coli* RecQ helicase. Almost
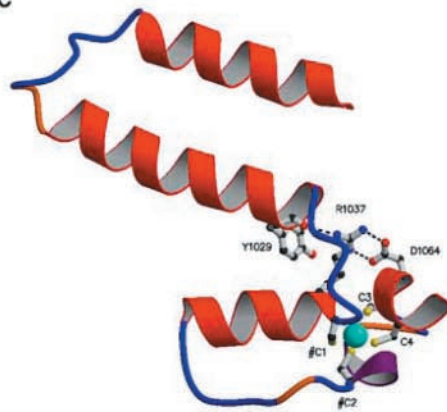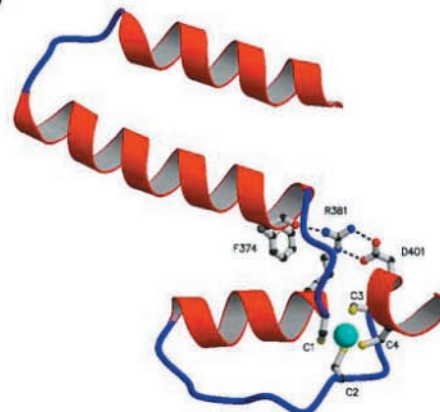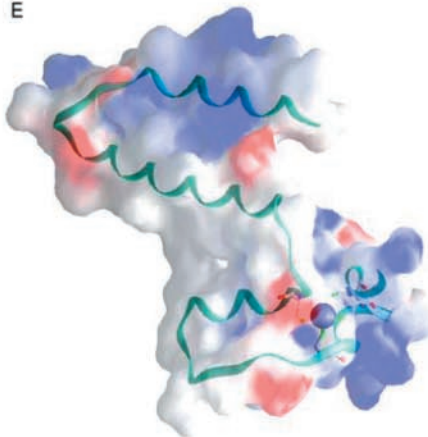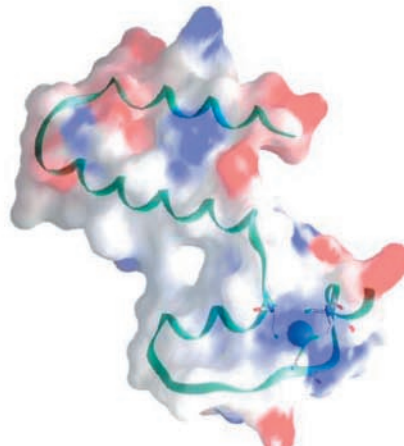
A

B

C   **D**

E   **F**

half of these 36 extra residues are found in the C-terminal portion of the model. More precisely, 16 residues are in the C-terminus, 10 are in the zinc binding domain and 10 residues are in the N-terminus. The enzyme is folded in four distinct domains, including a characteristic zinc binding domain. The root mean square deviation (RMSD) between the RecQ back-bones from *E.coli* and from the BS protein is 0.7 Å for 516 C_α atoms, the C-terminal region showing the most significant differences (Figure 2B). The overall topology of the zinc binding domain conforms to the expected fold of a classical C4 zinc binding domain which is composed of the four conserved cysteines: Cys-1036, Cys-1055, Cys-1063 and Cys-1066 (labelled C1–C4) bound to a single zinc ion (Figure 2C). In BLM, the zinc binding domain comprises 10 residues more than in *E.coli* (Figure 2A, C and D). They are divided into three main insertions (in orange in Figure 2C), the longer one between C2 and C3. Cys-1036 is in the conserved helix equivalent to α_{17} in RecQ model; Cys-1063 and Cys-1066 are located in the conserved helix equivalent to α_{18} in the RecQ model, in red in Figure 2C. The main differences appear in the region of the Cys-1055 residue (C2). Cys-1055 is located in a short α-helix, in violet in Figure 2C, situated between the helices equivalent to α_{17} and α_{18} in the RecQ structure. The restraint imposed by the proline and glycine residues surrounding C2 in the *E.coli* enzyme for positioning the cysteine side chain (Figure 2D) could be replaced by one helix in the BLM (in violet in Figure 2C). Due to this additional secondary structure element, it appears that all the cysteine residues bound to the Zn^{2+} ion are included into α-helices in the human enzyme. It is worth noting that two disease-associated mutations are found in the zinc binding domain. These mutations (indicated by # characters in Figure 2C) are C1036F at C1 position and C1055S at C2 position.

As in the RecQ template structure, the conformation of the BLM zinc binding domain is obviously stabilized through three hydrogen bonds (Figure 2C and D) between NE Arg-1037 and OD1 Asp-1064, NH2 Arg-1037 and OD2 Asp-1064, and between NH1 Arg-1037 and the main chain atom O of Tyr-1029, involving highly conserved residues in the RecQ family (Figure 2A). Arg-1037 is one residue after C1, and Asp-1064 is one residue after C3 whereas the equivalent of Tyr-1029 is always a tyrosine or phenylalanine positioned before C1. These three residues, involved in three hydrogen

bonds, contribute efficiently to the relative positioning of the α-helices of the zinc binding domain and thus appear to be important for the fold of this motif.

Interestingly, both zinc binding domains of BLM and *E.coli* RecQ helicase exhibit similar positively charged electrostatic surfaces (Figure 2E and F). It can be hypothesized that these positively charged regions could be involved in protein–protein or protein–DNA interactions (43).

Confirmation that BLM is a zinc-containing protein

To determine whether BLM binds a zinc ion, the zinc content of the purified helicase core of BLM was measured using PAR. As shown in Figure 3A, the increase in absorbance at 500 nm following BLM addition to a solution containing PAR indicates the formation of a PAR_2Zn^{2+} complex. Quantitative analysis of the amounts of zinc atom associated with the purified BLM indicated that the zinc atom binds to BLM in a stoichiometric ratio (Table 2). This observation was further confirmed by the existence of a linear correlation between the amount of zinc ion and the increasing concentration of the protein (Figure 3B). The slope value of 0.98 ± 0.11 indicates that each molecule of BLM contains one zinc ion. We then compared the number of solvent-accessible thiol groups between the full zinc-metalated and zinc-demetalated BLM. For this purpose, the zinc atom was removed from wild-type BLM by EDTA extraction (21). It is referred to, hereafter, as zinc-demetalated BLM helicase. With this EDTA extraction method, the content of the zinc atom of the zinc-demetalated BLM was reduced to 0.15–0.20 mol/mol enzyme. The results show that zinc-demetalated BLM has 2.85–3.12 additional solvent-accessible thiol groups. Considering the fact that the zinc extraction is incomplete and the presence of the inevitable partially oxidized protein, the above results are consistent with a zinc atom binding site being formed by four cysteines. These studies clearly show, in accordance with the modelled structure, that BLM carries a zinc binding domain.

Effect of the zinc ions on BLM enzymatic activities and on the conformational stability of the protein

The next question was whether the zinc ion binding to this protein is necessary for the DNA binding, ATPase and helicase

---

Figure 2. Modelled structure of the BLM helicase core and details of the sequence alignment. (**A**) Amino acid sequence alignment of the conserved putative zinc binding domain among the RecQ family helicases. The multiple alignments were performed with the program ClustalW and refined manually. The numbers at the beginning and the end of each sequence correspond respectively to the positions of the first and the last amino acid residues. Highly conserved amino acid residues are shadowed in grey. In red are the four conserved cysteine residues, labelled C1–C4, and, in blue, the fully conserved arginine, aspartic acid and aromatic residues, involved in three very important hydrogen bonds shown in (C). The consensus sequence was generated by ClustalW. The protein accession numbers used by the National Center for Biotechnology Information are RecQ, P15043 (*E.coli*); SgS1, P35187 (*S.serevisiae*); Rqh1, Q09811 (*Schizosaccharomyces pombe*); RecQL1, NP_002898/P46063 (*Homo sapiens*); WRN, NP_000544/Q14191 (*H.sapiens*); BLM, A57570/P54132 (*H.sapiens*); DmBLM, Q9VGI8 (*H.sapiens*); RECQL5, Q9BW80 (*H.sapiens*). Secondary structure elements of RecQ appear with boxes designing the α-helices of the zinc binding domain. (**B**) Stereo view of the Cα trace of the RecQ catalytic core from BS Protein (mauve), as obtained after refinement of the structure generated by the Modeller computation (see text for details) and superimposed with the catalytic core of *E.coli* RecQ (magenta) that served as template in the modelling. The root mean square deviation (RMSD) between the two structures is 0.7 Å for 516 Cα atoms. The zinc ion is in cyan. (**C**) Ribbon drawing of the zinc binding domain of the modelled BLM helicase core. The zinc ion is in cyan. Conserved α-helices are drawn in red whereas the three main insertions, compared with sequence from *E.coli*, are figured in orange. The modelled helix including C2 is drawn in violet. As in the alignment shown in (A), the positions of the four totally conserved cysteine residues are labelled as C1–C4. The fully conserved arginine, aspartic acid and aromatic residues, involved in three very important hydrogen-bonds (dashed lines) stabilizing the conformation of the zinc binding domain, are shown in ball and stick representation. (**D**) Ribbon drawing of the zinc binding domain in the crystal structure of the *E.coli* RecQ (PDB ID:1OWY). Colour codes and orientation are the same as in (C). In ball and stick are residues important for the structure and the function of the enzyme. (**E**) Grasp potential surface of the modelled BLM zinc binding domain in approximately the same orientation as in (C). The molecular surface is coloured by the electrostatic potential: blue, positive; red, negative; white, neutral and it is superimposed on the polypeptide chain. The Zn ion is in blue and C1–C4 cysteine residues appear in stick representation. (**F**) Grasp potential surface of *E.coli* zinc binding domain in the same orientation as in (D). The molecular surface is coloured by the electrostatic potential: blue, positive; red, negative; white, neutral and it is superimposed on the polypeptide chain. The Zn ion is in blue and C1–C4 cysteine residues appear in stick representation.
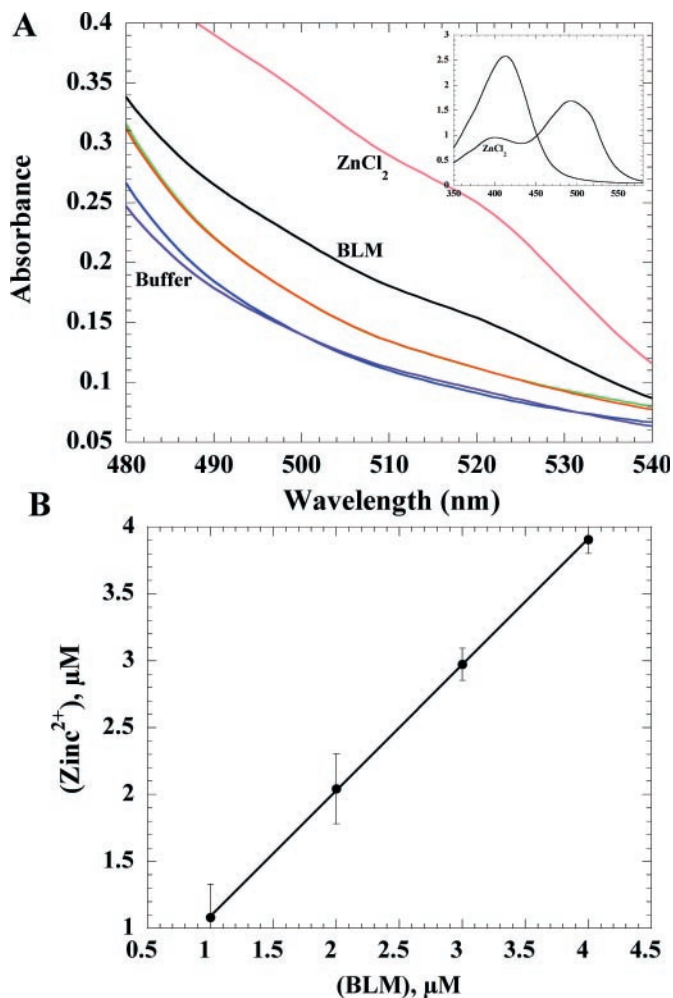
Figure 3. (**A**) Absorbance spectra of wild-type and mutant BLMs in the presence of PAR. Enzymes (1 nmol for wild-type and each mutant proteins) were prepared as indicated under Materials and Methods and were added to a 1 ml cuvette containing 100 μM PAR in Chelex®100-treated 50 mM Tris and 100 mM NaCl, pH 7.8. The spectra were scanned from 300 to 600 nm. As a control, 20 nmol ZnCl$_2$ was added and scanned in the same conditions. All assays were run at room temperature (25°C). From top to bottom: ZnCl$_2$, wild type, C1055N, C1063N, C1055N/C1063N and buffer alone. Inset: a typical absorbance spectra of PAR in the absence and in the presence of ZnCl$_2$. (**B**) Zinc ion quantity was determined as increasing concentration of the protein. The slope value of 0.98 determined from this figure indicates that the zinc atom binds to BLM protein in a stoichiometric ratio.

activities. The comparison of ATPase and helicase activities of wild type with that of the zinc-demetalated BLM helicase showed that BLM helicase can still hydrolyze ATP, bind DNA and unwind duplex DNA substrate in the absence of zinc ion. Parameters such as k_{cat} and K_m for ATPase and helicase activities display essentially the same values for the wild-type and zinc-demetalated enzymes (Table 2). The effect of the zinc atom on the enzymatic properties of wild-type and zinc-demetalated proteins was further evaluated with increasing zinc concentration. We found that the zinc ions only modestly affect ATPase activity of BLM (results not shown). Since the above observations might indicate that the zinc ion does not play an essential role in catalysis, we further investigated whether the zinc ion is important for the stability of BLM. This possible stabilization effect was substantiated by measuring ATPase activity at different temperatures. As shown in Figure 4A, the k_{cat} values of the zinc-demetalated BLM are systematically lower than that of the zinc-containing BLM, indicating that the zinc ion can enhance the thermostability of BLM. To confirm whether zinc stabilizes the conformation of BLM, we performed limited proteolysis on both heat-treated zinc-containing and zinc-demetalated BLMs. Figure 4B shows, in agreement with the thermostability experiments, that the zinc-demetalated BLM is less resistant to proteases than the zinc-containing BLM. Collectively, these results establish that the zinc ion is not implicated in catalysis, but plays an essential role in maintaining the stability of the 3D structure of the protein.

Characterization of BLM mutant proteins

Site-directed mutagenesis was used to elucidate the functional significance of the zinc binding domain. The design of mutations was based on three aspects of the structural and functional properties of BLM. First, according to molecular modelling, four cysteine residues are implicated in the zinc binding domain. Three of the four cysteine residues were therefore replaced by other residues. We attempted initially to make a panel of substitutions in which the four conserved cysteines would be replaced by four alanine or serine residues, but despite several attempts, we were not successful at generating these modified BLM proteins since these mutants appear to be degraded totally before the purification step even in the presence of protease inhibitors (PMSF, leupeptin and pepstatin). In contrast, mutant proteins with one or both positions at C$_2$ and

Table 2. Properties of wild-type and mutated BLM proteins

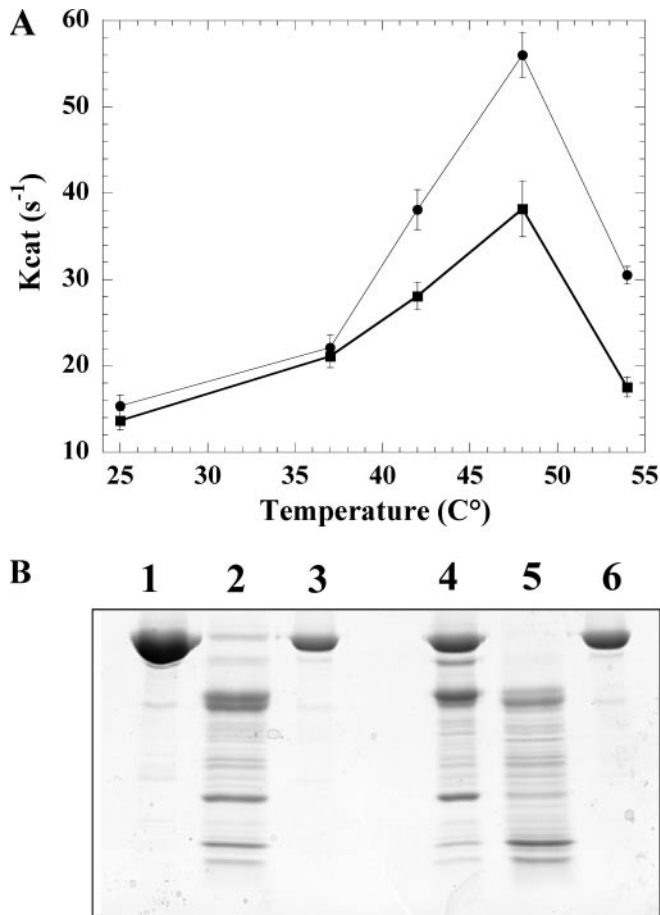| Protein	Proteins state[a]	Zinc[b]	ATPase activity (s^{-1})				Helicase activity		DNA binding (nM)		ATP binding (μM)	R_s[c] (Å)
			k_{cat}	$k_{cat}^{wt}/k_{cat}^{mut}$	K_m (μM)	k_m^{mut}/k_m^{wt}	k_{cat}	$k_{cat}^{wt}/k_{cat}^{mut}$	K_d^{dsDNA}	K_d^{G4DNA}	K_d (μM)	
WT	S	0.98	26.48	1	88	1	2.5×10^{-2}	1.00	29.8 ± 1.3	4.57	50.26 ± 0.71	34.57
WT^{zn-}	S	0.18	28.56	0.95	79	1	2.6×10^{-2}	0.96	30.5 ± 2.5	4.85	52.3 ± 0.95	33.87
C1055N	S	0.50	1.15	22.95	938.5	10.61	0.9×10^{-2}	2.7	56 ± 1.8	400	78.65 ± 6.5	33.98
C1063N	S	0.52	2.16	12.26	3149	35.57	5.4×10^{-4}	46.3	124 ± 2.3	1986	64.47 ± 1.9	34.69
C1055N/C1063N	S	0.01	4.26	6.21	6648	75.07	9.9×10^{-4}	25.5	209 ± 3.5	3.28×10^{15}	100.6 ± 3.7	34.94
C1036F	I						ND[d]					
C1055S	D						ND					
R1037A	I						ND					

[a]S, D and I represent soluble protein, degraded protein and protein in the form of inclusion bodies.
[b]These values represent the number of zinc ion per molecule of protein.
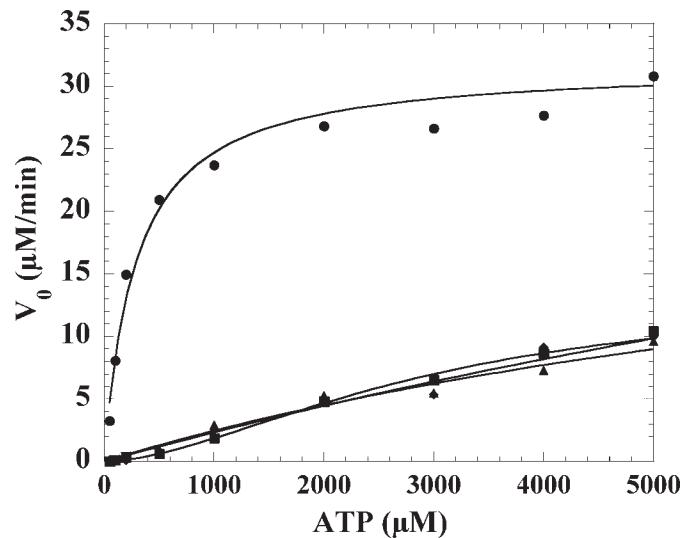[c]R_s represent Stokes radii.
[d]ND, non determined.

Figure 5. ATP hydrolysis activity of wild-type and mutant BLMs as a function of ATP concentrations. Experiments were performed in ATPase assay buffer (25 mM Tris–HCl; 35 mM NaCl; 0.5 mM DTT and 3 mM $MgCl_2$) at $37°C$ with 6 µM ssDNA (nt, 60mer oligonucleotide) and 10 nM protein for each enzyme. The ATP hydrolysis was quantified as described in Materials and Methods. The lines correspond to the fits to a Michaelis–Menten equation for wt (circle), C1063N mutant (triangle), C1055N (square) and C1055N/C1063N (rhombus). The apparent k_{cat} and K_m values are presented in Table 2.

Figure 4. (**A**) ATPase activity of BLM[642–1290] and zinc-demetalated BLM[642–1290] as a function of temperature. ATPase activity was assayed in the presence of 10 nM BLM with increasing concentration of ATP at the indicated temperatures. The experimental data were analysed according to the Michaelis–Menten equation, and the apparent k_{cat} and K_m values were determined from the best fit. (**B**) Limited proteolysis of BLM and zinc demetalated BLM. Both BLM (lanes 1 and 4) and zinc demetalated BLM (lanes 2 and 5) (15 µg for each protein) were incubated at $48°C$ for 5 min, and were digested with 0.065% (lanes 1 and 2) and 0.12% (lanes 4 and 5) trypsin (w/v) at $4°C$ for 3 min. The reaction was stopped by addition of PMSF to a final concentration of 10 mM. The samples were separated by SDS–PAGE and stained with Coomassie blue. Lane 3 is BLM control (10 µg, not heat-treated, not digested).

C_3 replaced by asparagine were purified to homogeneity. Their ability to bind zinc was therefore assessed under the same experimental conditions, as the wild-type enzyme. While 0.95 mol of zinc ion was bound to 1 mol of the wild-type enzyme, only 0.50, 0.52 and 0.01 mol zinc ion was bound to the mutants C1055N, C1063N and to the double mutant C1055N/C1063N, respectively (Table 2). Second, the modelled structure suggests that Arg-1037, Asp-1064 and Tyr-1029 could be involved in hydrogen bonds, and could contribute to the stabilization of the zinc motif. We therefore investigated the role of these residues in the stabilization of the protein conformation. In fact, a previous study has shown that replacement of D1064 by alanine severely impaired the helicase and DNA binding activities (34). We thus speculated that the mutant R1037A could display similar properties as the mutant D1064A. Surprisingly, the resulting mutant R1037A was completely degraded before purification, pre-

venting its study. These results indicate that both Arg-1037 and Asp-1064 stabilize the structure of the zinc binding domain and of the whole protein, a topic that will be further discussed in the Discussion. Third, two point mutations C1055S and C1036F have been previously identified in human BS patients (20,22). To understand the impact of these residues on the zinc binding domain together with the molecular and structural basis of this disease, Cys-1055 was replaced by serine and Cys-1036 was replaced by phenylanine, respectively. The resulting mutants either displayed a high level of susceptibility to degradation (C1055S) or formed inclusion bodies (C1036F) (Table 2), making it impossible to purify the proteins for further analysis.

These results, taken together, indicate that BLM contains a functional zinc motif that coordinates a single, tetrahedral Zn^{2+} ion using the four conserved cysteines. The zinc binding domain could be further stabilized by hydrogen bonds formed between Y1029 and R1037 and between R1037 and D1064.

The zinc binding domain is required for ATPase and helicase activities

The functional significance of the zinc binding motif was assessed by measuring ATPase and helicase activities of the wild-type and mutant proteins. ATPase activity was measured in the presence of DNA to stimulate the ATP hydrolysis activity of BLM. While the wild-type protein displayed an ATPase activity that remains comparable with the previous determination $(35\,s^{-1})$, this activity was severely modified for the mutant proteins (Figure 5). Compared with wild-type enzyme, the k_{cat} values for mutant proteins decreased from 6- to 25-fold, and the K_m values increased from 10- to 74-fold.

The helicase activity of wild-type and of the mutant proteins were analysed on a partial DNA duplex substrate comprising a

44mer radiolabelled oligonucleotide annealed to a 45mer oligonucleotide. This substrate was incubated with increasing amounts of BLMs in the presence of ATP, followed by analysis of the reaction products on a non-denaturing 15%

polyacrylamide gel. Results given in Figure 6A indicate that the mutant proteins do not or poorly unwind DNA substrates. This led us to determine the apparent k_{cat} values of helicases using a fluorescence assay under equilibrium conditions.
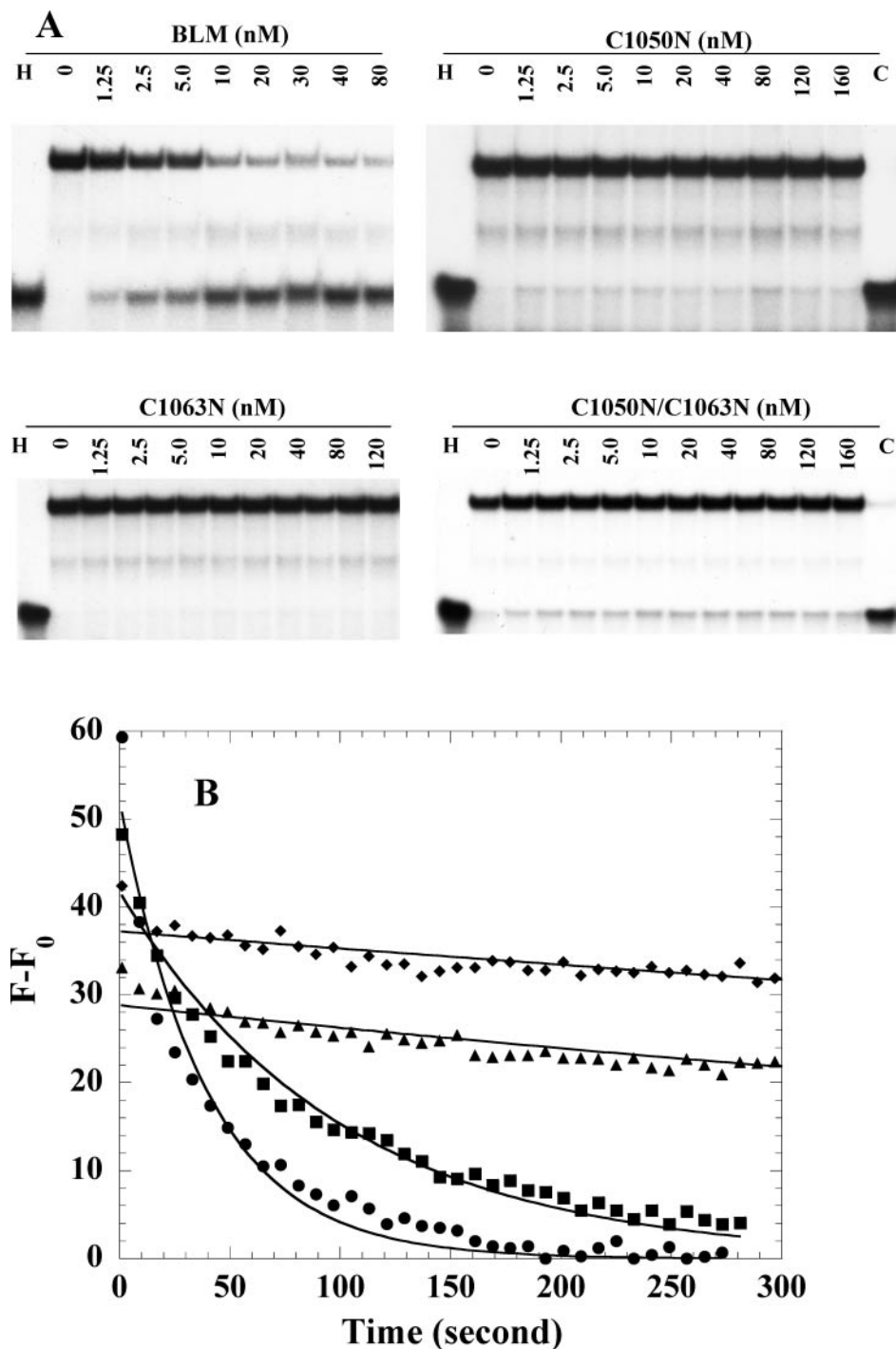
Figure 6. (**A**) DNA helicase activity of BLM[642–1290] and mutant proteins revealed by radiometric assay. 5′-^{32}P-labelled DNA substrate was incubated at 30°C with BLM[642–1290] and different point mutants in the helicase assay buffer. The reactions were terminated after 30 min and the samples were analysed by electrophoresis in a 10% non-denaturing polyacrylamide gel. The concentrations of the proteins range from 1.25 to 160 nM. The H represents the heat-denatured substrate control, and the C represents the BLM[642–1290] enzyme control. (**B**) Kinetic analyses of DNA unwinding by wild-type BLM (circle) and mutant proteins (triangle, C1055N; rhombus, C1063N; square, C1055N/C1063N) using a fluorometric assay. Helicase reaction mixtures contained 1 nM partial duplex DNA substrate in unwinding buffer. DNA unwinding was initiated with addition of 1 mM ATP at 25°C. Data from the time courses were fitted to the exponential equation: $A_t = A \exp(-k_{obs}t)$, where A_t is the anisotropy amplitude at time t, and k_{obs} is the observed rate constant. These data are summarized in Table 2.

Figure 6B shows that, consistent with the previous results obtained with the gel shift method, the mutants C1050N and C1063N display only very weak helicase activities. The k_{cat} values were decreased to 35- and 74-fold for the mutant C1055N and the mutant C1063N, respectively. Surprisingly, the k_{cat} value for the mutant C1055N/C1063N was only decreased 3-fold compared to that of wild-type enzyme. These results, collectively, indicate that the zinc binding domain is crucial to ATPase and helicase activity of BLM.

Mutation of cysteine residues implicated in the zinc binding domain does not affect ATP binding

To further improve our understanding on the role of the zinc binding domain in BLM, ATP binding by the wild-type and mutant proteins was examined by UV cross-linking, as previously reported (29). Both purified wild-type and mutant proteins were incubated with [γ-^{32}P]ATP. The mixtures were subsequently cross-linked via UV light. Proteins that display ATP binding activity are covalently bound to ATP and thus become radiolabelled. Both wild-type and mutant helicase proteins were efficiently labelled, as illustrated in Figure 7A. No radioactivity was observed, however, if the mixture was not exposed to UV light or if BSA protein was used in place of the helicase protein, thus revealing specific binding of ATP to the helicase protein. However, this is a non-equilibrium method. We therefore studied ATP binding quantitatively using mantATP as a fluorescent ATP analogue under equilibrium conditions. Mant-nucleotides are widely used with many NTPases for investigating nucleotide binding because the spectral properties of mant-fluorescence are ideally suited for monitoring nucleotide binding by FRET (23,30). We first confirmed that the emission spectrum of BLM overlaps with the excitation spectrum of the mantATP, indicating the possibility of performing FRET (Figure 7B). The apparent association constant values (K_d) of mantATP for wild-type and mutant proteins were determined over increasing concentrations of mantATP (Figure 7C). The values for the wild-type and mutant proteins were found to be similar (Table 2). This study shows therefore that the zinc ion and the zinc binding domain are not required for ATP binding.
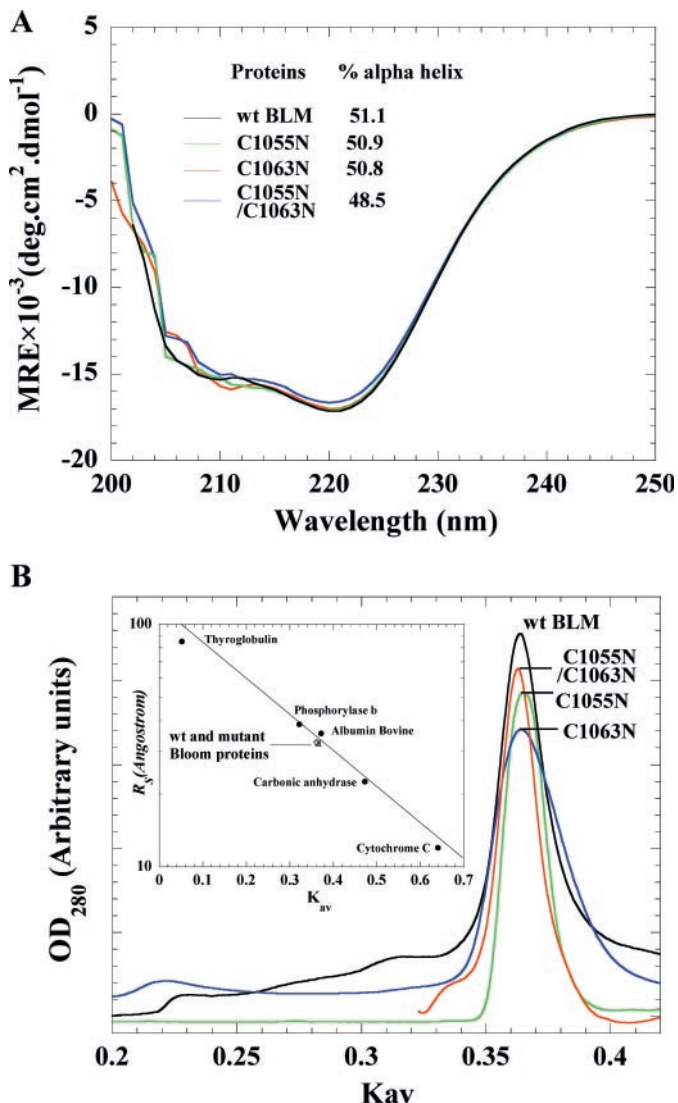
Structural characterization of the mutant proteins

To determine whether the mutations induce a change in protein conformation, and consequently affect its activity, we characterized some of the structural properties of the mutant enzymes with two different approaches. Far-UV CD was first used to analyse the secondary structure of the proteins. The CD spectra of both wild-type and mutant proteins show a maximum at ~200 nm and two strong minima at 208 and 222 nm, characteristic of α-helical structures (Figure 8A). Analysis of the CD spectra using % α-helices = $\Delta\varepsilon_{222nm} \times (-10)$ indicate that wild-type BLM contains ~51.1% α-helical structure, in agreement with the secondary structure prediction data (50.5% α-helices, see Supplementary Material). The three mutant proteins displayed only a modest reduction in α-helices content, presenting 50.9, 50.3 and 48.5% α-helical structure for C1055N, C1063N and C1055N/C1063N, respectively. Thus, the replacement of one cysteine residue within the zinc binding domain does not produce significant change in the
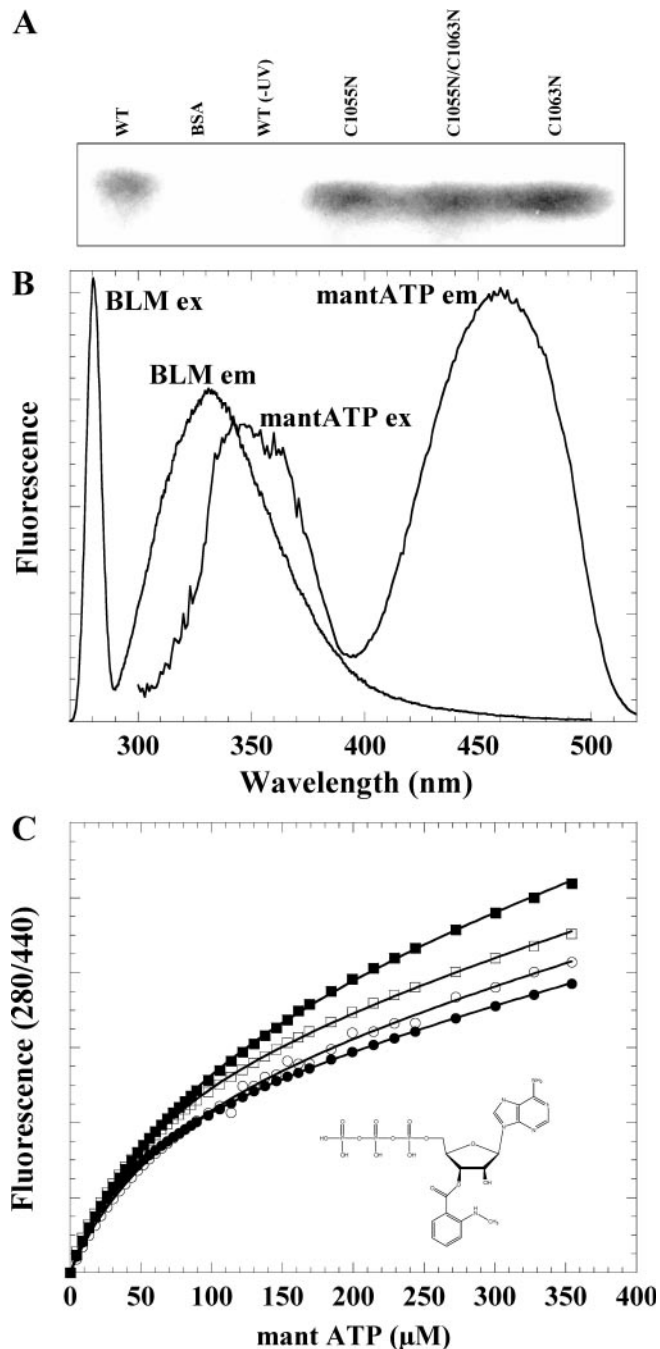
Figure 7. (**A**) ATP binding activity of the wild-type (BLM$^{642-1290}$) and mutant BLMs. One microgram of the wild-type or mutant helicase protein was incubated with [γ-^{32}P]ATP in the presence of ssDNA (60 base) and was UV cross-linked as described under Materials and Methods. Samples were separated by SDS–8% PAGE. Following electrophoresis, the gels were stained with Coomassie brillant blue, dried and processed for autoradiography. WT, wild-type BLM (BLM$^{642-1290}$); WT (−UV), wild-type enzyme not exposed to UV; BSA, bovine serum albumin. (**B**) The overlap of the BLM emission spectrum (λ_{ex} = 280 nm) and the mantATP excitation spectrum (λ_{em} = 440 nm). The excitation wavelength for the mantATP emission spectrum is λ_{ex} = 345 nm. For the reason of clarity, only wild-type BLM protein excitation-emission spectrum is shown. (**C**) Changes in fluorescence intensity when 0.5 μM wild-type (open squares), and mutant proteins (C1055N, closed circle; C1063N, closed square; open circle, C1055N/C1063N) were titrated with increasing concentration of mantATP. Solid lines represent the best fit of the data to Equation 1 and the apparent K_d values are summarized in Table 2. Molecular structure of mantATP is shown in the insert.

Figure 8. Structural characterization of the mutant BLMs. (**A**) Normalized CD spectra of wild-type and different mutant BLMs (indicated in the figure). The experiments were performed as described under Materials and Methods. About 8 μM of each protein was used in this experiment. All of the spectra are given in units of MRE. (**B**) Analysis of wild-type and mutant BLM proteins by size exclusion chromatography. Experiments were performed at room temperature using a Superdex 200 column. Shown are the elution profiles of wild-type and mutant proteins as indicated in the figures. About 5 μM protein was used for each experiment. Insert: The molecular weight calibration to the partition coefficient K_{av}, using protein molecular weight standards (closed circle), as indicated under Materials and Methods. The open symbols indicate the positions of wild-type and mutants proteins.

secondary structure of the BLM protein as judged from the CD spectra.

Size exclusion chromatography was used to determine the Stokes radius of wild-type and mutant proteins. Figure 8B shows that both wild-type and mutant proteins were found to elute in a single peak corresponding to a molecular mass of 71 600 Da, a value close to the predicted molecular mass (74.1 kDa). These results not only confirm that BLM and its modified versions exist as a monomer in solution, but also reveal that the Stokes radius values of the wild-type and mutant proteins are very similar (∼35 Å, Table 2), indicating that

the overall structure of these mutants is close to that of wild type. The above results show that the wild-type and the mutant helicases fold into similar 3D structures.

Zinc binding domain and DNA binding

Having established that the wild-type and mutant proteins display the same affinity for ATP and are folded similarly, we then characterized the DNA binding activity of the wild-type and mutant BLM helicases, using the electrophoretic mobility shift assay. Compared with the DNA binding ability of the wild-type BLM, that of the mutant proteins is severely modified. As shown in Figure 9A, the C1055N mutant and the C1055N/C1063N double mutant display severely reduced, but still detectable, DNA binding activities. In addition, the DNA binding activity of the C1063N mutant is completely compromised. From the above observation, namely that the C1063N mutant displays a detectable ATPase activity, we reasoned that the C1063N mutant could retain a weak DNA binding activity, but not strong enough to be detected by electrophoresis mobility shift assays. The apparent K_d values of both wild-type and mutant proteins were thus determined under equilibrium conditions, using fluorescence anisotropy assays (25). Figure 9B shows that all the mutants display a reduction in their affinity for DNA compared to the wild-type BLM, the values ranging from ∼2.6-fold decrease (in apparent K_d) for the C1055N/C1063N mutant to >7-fold decrease for the C1063N mutant. The above results suggest that the zinc binding domain plays an important role for DNA binding of BLM. Previous experiments have shown that G-quadruplex DNA (G4 DNA) is a preferred substrate over canonical Watson–Crick duplexes for BLM (9). To investigate whether the zinc binding domain is involved in G4 DNA recognition and binding, we compared the binding of the wild-type and the mutant proteins to G4 DNA. Figure 10 shows that the binding of the mutants is severely impaired when compared with that of the wild-type BLM. Interestingly, while the binding activity of the mutant C1055N for the duplex DNA is only reduced, it is almost abrogated for the G4 DNA, indicating that the zinc binding domain plays an important role in the specific binding of BLM to G4 DNAs. These data allow us to conclude that the zinc binding domain is strongly involved in DNA binding, and especially in G4 DNA binding.

DISCUSSION

Our data demonstrate that the evolutionarily conserved RecQ-Ct region of BLM forms a zinc binding domain. We present also evidence that the zinc binding domain plays an essential role in DNA binding, protein stability and protein folding. These observations shed light on the question of how some missense mutations can lead to the destabilization of the genome and ultimately to tumorigenesis, and provide an explanation of the molecular basis of BS pathogenesis.

BLM harbours a zinc binding domain

Zinc binding domains are abundant in the genomes of eukaryotic organisms. It is estimated that ∼3% of all human gene products contain one or more zinc-binding domains or zinc fingers. They are known to be involved in protein–DNA interactions, protein–protein interactions, as well as protein folding
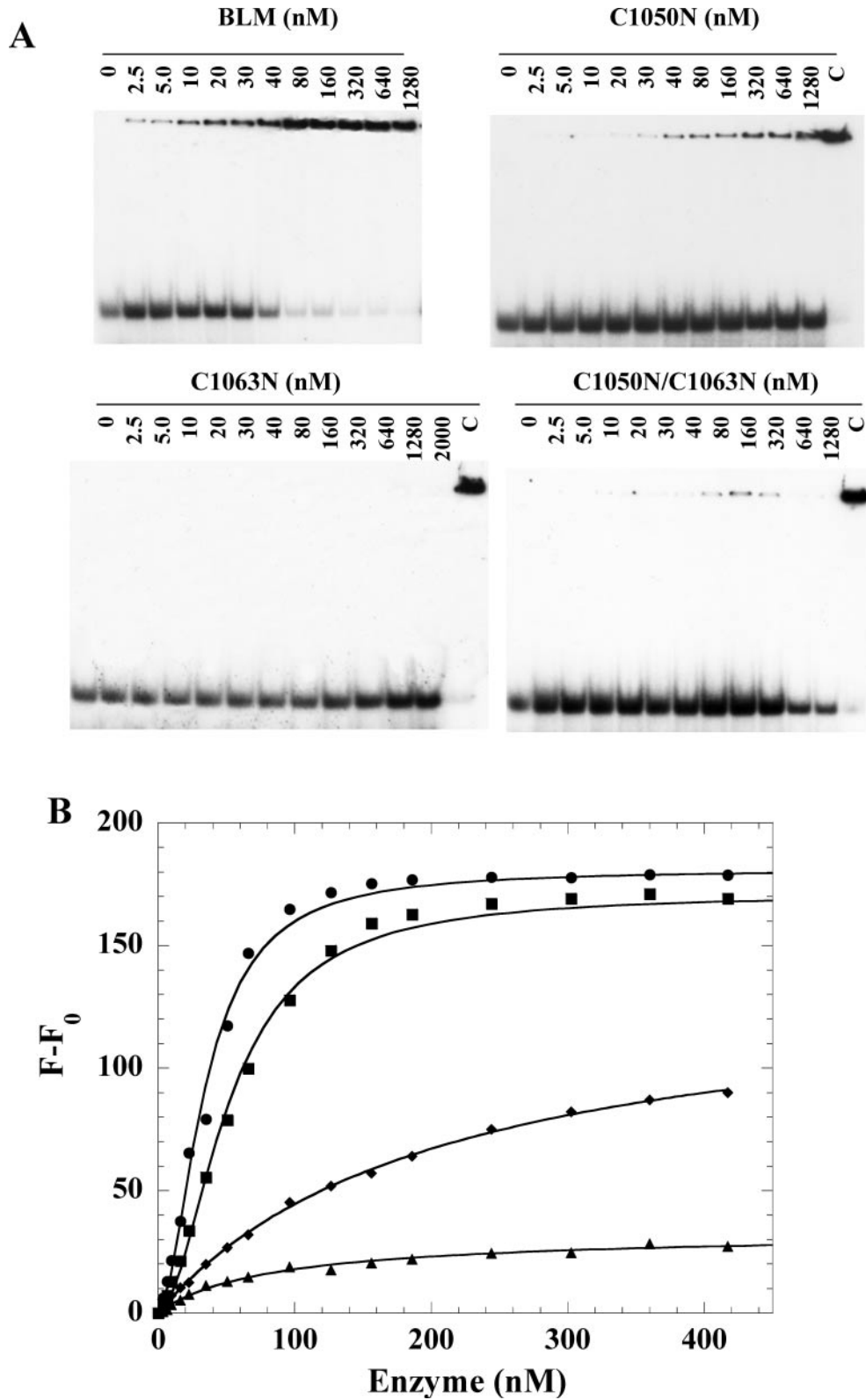
Figure 9. (**A**) Analyses of DNA binding activity of wild-type and mutant BLMs using electrophoretic mobility shift assay. One nanomole of 5′-end-labelled duplex DNA was incubated at room temperature for 20 min with different concentration of the proteins varying from 2.5 to 2000 nM in unwinding buffer. Bound and free DNA were separated by electrophoresis through a non-denaturing 15% polyacrylamide gel and visualized by autoradiograph. The C represents the wild-type control. (**B**) DNA binding to the wild-type (circle) and mutant proteins (C1050N, square; C1063N triangle; C1055N/C1063N, rhombus) under equilibrium condition. The anisotropy based binding isotherms were obtained upon titration of the 3′-fluorescence-labelled DNA substrate which is identical to the DNA used in radiometric assay, except it is not 5′-^{32}P-end-labelled. The DNA binding isotherms were fitted to a Michaelis–Menten equation. The apparent K_m values are presented in Table 2.
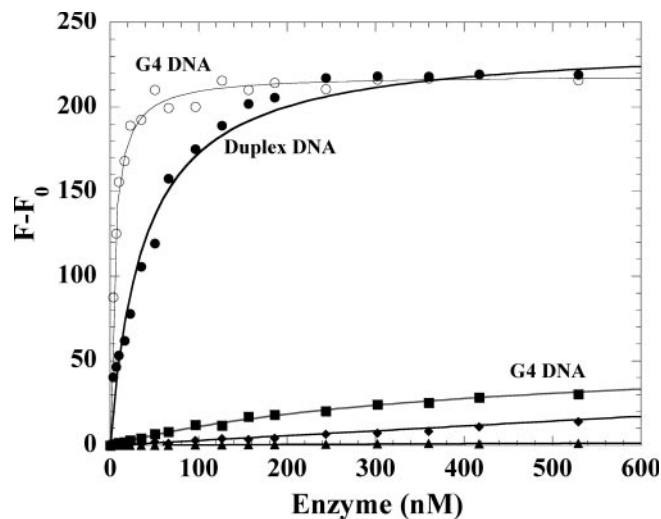
Figure 10. G-quartet DNA binding activity for BLM protein is severely impaired upon the zinc binding domain mutations. Two nanomoles 5′-fluorescein labelled G4 DNA and duplex DNA were titrated with the wild-type BLM (open and closed circle, respectively) and the mutated enzymes (C1063N, triangle; C1055N, square; C1055N/C1063N, rhombus) under the same experimental conditions as indicated in Figure 9B. Note that while the wild-type BLM displays higher affinity for G4 DNA over the duplex DNA (Figure 9B), the binding affinity for G4 DNA is greatly reduced for the three mutants, especially for the C1055N mutant (square).

(43–45). Previous sequence analyses have shown that BLM may contain a protein sequence reminiscent of a zinc finger DNA binding domain (20). This suggestion became more persuasive when a zinc binding domain was identified in the C-terminal domain of *E.coli* RecQ helicase, a domain conserved by sequence homology in BLM (21). However, direct experiments designed to confirm the existence of such a zinc binding domain and to explore its function in BLM were still lacking. In this study, a combination of molecular modelling, site-directed mutagenesis, and biochemical and biophysical analyses indicate that the BLM RecQ-Ct domain harbours a functional zinc binding domain. Theoretical prediction suggested the potential of this region to form a tightly folded zinc binding module. This theoretical consideration provides a structural rationale for exploring the function of the zinc binding domain in BLM. Although only X-ray crystallography and/or multidimensional NMR spectroscopy can precisely define the details of the 3D structure of this motif, the lines of evidence reported here confirm that the zinc ion is ligated by four conserved cysteines. (i) The PAR assay clearly shows that the zinc ion binds to BLM in a stoichiometric fashion. (ii) Comparison of the solvent-accessible thiol groups in the fully zinc-metalated and the zinc-demetalated proteins indicates that the zinc atom binding site is comprised of four cysteines. (iii) Site-directed mutagenesis studies confirm that the four cysteine residues are implicated in binding the zinc ion. In addition, a careful analysis of the zinc-demetalated BLM indicated that the zinc ion is not directly implicated in ATPase, helicase or DNA binding activities. However, this ion appears very important for the precise folding of the zinc binding domain and consequently for maintaining protein stability. Once the protein is correctly folded, the presence of the zinc ion is not absolutely required for the enzymatic activities but is required for protein structure

stability. This agrees with the previous observation that metal ions play an essential role in the protein folding process for the formation of secondary and tertiary structures, whereas the demetalated proteins still keep a well-defined tertiary structure and function (48).

Functional significance of the zinc binding domain in BLM

The functional importance of the zinc binding domain was evaluated by comprehensive site-directed mutagenesis, and by biochemical and biophysical approaches. Altering one of the four conserved cysteines was found to severely reduce or abrogate ATPase and helicase activities. There are several possible explanations for these defects. First, alteration of one of the four cysteine residues may impair ATP binding, leading to a loss in enzymatic activity. This possibility is excluded by our ATP binding studies. Moreover, UV cross-linking experiments showed that the mutant proteins were as efficiently labelled as the wild-type enzyme. This was confirmed by quantitative binding studies performed under equilibrium conditions, where both mutant and wild-type enzymes displayed very similar apparent K_d values for mantATP. An alternative possibility is that the alteration of the cysteine residues implicated in the zinc binding domain provokes an overall conformational change resulting in the observed defects in the enzymatic activities. However, both CD and size-exclusion chromatography data indicated that mutations do not entail gross conformational changes. The other possibility would be that these mutations lead to subtle and localized conformational changes, these being sufficient to result in loss of DNA binding activities. We observed that the DNA binding abilities of the mutants are severely reduced or almost abolished when one of the four cysteine residues was altered. Since the BLM helicase is a DNA-stimulated ATPase and ATP-dependent helicase, it appears that the defect of DNA binding could be the primary effect of the mutations. We therefore conclude that the zinc binding domain of BLM is strongly involved in DNA binding.

Two hypotheses can be put forward to explain how the zinc binding domain is implicated in DNA binding. First, the zinc binding domain could directly contact the DNA. Our modelled BLM structure shows that the zinc binding domain is folded into five α-helices, which are tightly packed together. In this defined structure, some residues could have a spatial configuration allowing a direct interaction with DNA. Alternatively, the zinc binding domain could also be indirectly implicated in the DNA binding. According to our modelled BLM structure and the *E.coli* RecQ helicase crystal structure, the zinc binding domain separates the helicase core and the C-terminal domain which has been suggested to play a role in DNA binding. As the helicase core is essential for the unwinding activity, it must also be involved in DNA binding. The interplay between the helicase domain and the C-terminal domain may be finely tuned by the zinc binding domain to ensure a precise DNA binding. Therefore, the mutations performed in the zinc binding domain could alter the relative orientation of these domains and may consequently have indirect but profound effects on DNA binding.

However, ensuring correct protein folding could be another potential function of the zinc binding domain of BLM. It is

worth to note that many mutations altering the zinc binding domain could not be purified due to extensive proteolytic degradation. In this way, the alteration of the conserved cysteine residues could lead to an incorrectly folded or partially denatured protein that is very sensitive to protease degradation. These observations are reminiscent of *E.coli* RecQ helicase and are coincident with the observations by Janscak *et al*. (34), showing that all the three cysteine to alanine mutants they made displayed a high level of susceptibility to proteolytic degradation (23). The zinc binding domain may function in the BLM folding cascade, favouring the link between the domains and the stabilization of the protein's conformation. Furthermore, Janscak *et al*. also observed that the replacement of D1064 by alanine entailed a dramatic reduction of both DNA binding and helicase activity, while replacement of D1064 with asparagine kept the properties of the mutant similar to the wild type, in terms of DNA binding and helicase activity. These observations are also consistent with our theoretical BLM model which shows that the hydrogen bonds between R1037 and D1064 are crucial for stabilizing the structure of the zinc binding domain, and therefore the whole protein structure. Replacement of Asp-1064 with the non-polar residue alanine should certainly completely disrupt the interactions between residues 1037 and 1064. In accordance with this reasoning, the replacement of R1037 with alanine in our studies resulted in protein degradation even in the presence of protease inhibitors, suggesting that the hydrogen bond between R1037 and D1064 plays an important role in the conformational stabilization of BLM. Moreover, the mutant R1038A exhibits very low activities in both DNA binding and DNA unwinding (34). These results indicate that, in addition to the four cysteine residues, a cluster of amino acids in the zinc binding domain could participate to the stabilization of the protein structure. Thus, the zinc binding domain of BLM appears to play a dual role in maintaining the structural and functional integrity of the BLM protein and in playing a pivotal role in DNA binding.

Implication for pathology

Many of the mutations found hitherto at the *BLM* locus that are associated with BS either create a stop codon mutation or cause a frame shift that leads to premature termination, which are predicted to eliminate the function of one or more of the helicase motifs. However, there are two point mutations mapping to Cys-1036 and Cys-1055, which lie outside of the conserved helicase motifs. Is it possible that these two point mutations also inactivate the helicase function of BLM or severely impair its enzymatic activities? To address these questions, we produced the two disease-linked missense mutations found in patients, C1036F and C1055S. One of these mutant proteins, C1055S, was completely degraded before the purification step and the other one, C1036F, precipitated during the biosynthesis, by forming an inclusion body (Table 2). Therefore, it was not possible to further characterize these mutations directly. However, a previous study on the murine C1063S mutant BLM has shown it to be defective in helicase and ATPase activities (46). Another study performed with human BLM has shown that the cells expressing the C1055S allele present a diffuse nuclear distribution of this missense BLM as well as a severe reduction in both helicase

and ATPase activities (47). These results, together with the above observations, shed light on the molecular basis of the two disease-linked BLM missense mutations. First, it seems possible that these mutations severely modify the 3D structure of the protein, resulting in its degradation or precipitation, and therefore the abrogation of all the enzymatic activities. Second, it is possible that, in the human cell context, the mutant proteins could exist as soluble protein due to chaperone or protein–protein interactions. However, as shown above, the soluble mutants resulting from altered cysteine residues display drastically reduced or completely abolished DNA binding and enzymatic activities. Finally, the combination of the above-mentioned events could lead to the disease. This alteration of the zinc binding domain should dramatically modify the protein structure and function, leading to BS.

Previous studies have shown that mutations or deletions in the C-terminal part of BLM have a dominant negative effect on the SCE frequency and cause an increase in chromosome abnormalities (15). The data presented in this paper further emphasize the importance of the C-terminal domain in BLM function, including DNA binding. The C-terminal domain may confer BLM the ability to recognize and bind abnormal DNA structures such as quadruplexes (G4 DNA) (9). This is consistent with our observation that some mutations in the zinc binding domain completely impair the binding to G4 DNA while binding to the duplex DNA is still detectable. The possible direct implication of the zinc binding domain in the binding of BLM to the G4 DNA is currently under investigation in our laboratory.

REFERENCES

1. German,J., Roe,A.M., Leppert,M.F. and Ellis,N.A. (1994) Bloom syndrome: an analysis of consanguineous families assigns the locus mutated to chromosome band 15q26.1. *Proc. Natl Acad. Sci. USA*, **91**, 6669–6673.
2. German,J., Crippa,L.P. and Bloom,D. (1974) Bloom's syndrome. III. Analysis of the chromosome aberration characteristic of this disorder. *Chromosoma*, **48**, 361–366.
3. German,J. (1993) Bloom syndrome: a Mendelian prototype of somatic mutational disease. *Medicine (Baltimore)*, **72**, 393–406.

4. Hickson,I.D., Davies,S.L., Li,J.L., Levitt,N.C., Mohaghegh,P., North,P.S. and Wu,L. (2001) Role of the Bloom's syndrome helicase in maintenance of genome stability. *Biochem. Soc. Trans.*, **29**, 201–204.

5. Karow,J.K., Chakraverty,R.K. and Hickson,I.D. (1997) The Bloom's syndrome gene product is a 3′–5′ DNA helicase. *J. Biol. Chem.*, **272**, 30611–30614.

6. Lohman,T.M. and Bjornson,K.P. (1996) Mechanisms of helicase-catalyzed DNA unwinding. *Annu. Rev. Biochem.*, **65**, 169–214.

7. Wu,L., Davies,S.L., Levitt,N.C. and Hickson,I.D. (2001) Potential role for the BLM helicase in recombinational repair via a conserved interaction with RAD51. *J. Biol. Chem.*, **276**, 19375–19381.

8. Fry,M. and Loeb,L.A. (1999) Human werner syndrome DNA helicase unwinds tetrahelical structures of the fragile X syndrome repeat sequence d(CGG)$_n$. *J. Biol. Chem.*, **274**, 12797–12802.

9. Sun,H., Karow,J.K., Hickson,I.D. and Maizels,N. (1998) The Bloom's syndrome helicase unwinds G4 DNA. *J. Biol. Chem.*, **273**, 27587–27592.

10. Mohaghegh,P., Karow,J.K., Brosh,J.R.,Jr, Bohr,V.A. and Hickson,I.D. (2001) The Bloom's and Werner's syndrome proteins are DNA structure-specific helicases. *Nucleic Acids Res.*, **29**, 2843–2849.

11. Karow,J.K., Constantinou,A., Li,J.L., West,S.C. and Hickson,I.D. (2000) The Bloom's syndrome gene product promotes branch migration of Holliday junctions. *Proc. Natl Acad. Sci. USA*, **97**, 6504–6508.

12. Brosh,R.M.,Jr, Majumdar,A., Desai,S., Hickson,I.D., Bohr,V.A. and Seidman,M.M. (2001) Unwinding of a DNA triple helix by the Werner and Bloom syndrome helicases. *J. Biol. Chem.*, **276**, 3024–3030.

13. Wu,L. and Hickson,I.D. (2003) The Bloom's syndrome helicase suppresses crossing over during homologous recombination. *Nature*, **426**, 870–874.

14. Liu,Z., Macias,M.J., Bottomley,M.J., Stier,G., Linge,J.P., Nilges,M., Bork,P. and Sattler,M. (1999) The three-dimensional structure of the HRDC domain and implications for the Werner and Bloom syndrome proteins. *Structure Fold. Des.*, **7**, 1557–1566.

15. Yankiwski,V., Noonan,J.P. and Neff,N.F. (2001) The C-terminal domain of the Bloom syndrome DNA helicase is essential for genomic stability. *BMC Cell Biol.*, **2**, 11.

16. Wang,Y., Cortez,D., Yazdi,P., Neff,N., Elledge,S.J. and Qin,J. (2000) BASC, a super complex of BRCA1-associated proteins involved in the recognition and repair of aberrant DNA structures. *Genes Dev.*, **14**, 927–939.

17. Brosh,R.M.,Jr, Li,J.L., Kenny,M.K., Karow,J.K., Cooper,M.P., Kureekattil,R.P., Hickson,I.D. and Bohr,V.A. (2000) Replication protein A physically interacts with the Bloom's syndrome protein and stimulates its helicase activity. *J. Biol. Chem.*, **275**, 23500–23508.

18. Wu,L., Davies,S.L., North,P.S., Goulaouic,H., Riou,J.F., Turley,H., Gatter,K.C. and Hickson,I.D. (2000) The Bloom's syndrome gene product interacts with topoisomerase III. *J. Biol. Chem.*, **275**, 9636–9644.

19. Johnson,F.B., Lombard,D.B., Neff,N.F., Mastrangelo,M.A., Dewolf,W., Ellis,N.A., Marciniak,R.A., Yin,Y., Jaenisch,R. and Guarente,L. (2000) Association of the Bloom syndrome protein with topoisomerase IIIalpha in somatic and meiotic cells. *Cancer Res.*, **60**, 1162–1167.

20. Langland,G., Kordich,J., Creaney,J., Goss,K.H., Lillard-Wetherell,K., Bebenek,K., Kunkel,T.A. and Groden,J. (2001) The Bloom's syndrome protein (BLM) interacts with MLH1 but is not required for DNA mismatch repair. *J. Biol. Chem.*, **276**, 30031–30035.

21. Sharma,S., Sommers,J.A., Wu,L., Bohr,V.A., Hickson,I.D. and Brosh,R.M.,Jr (2004) Stimulation of flap endonuclease-1 by the Bloom's syndrome protein. *J. Biol. Chem.*, **279**, 9847–9856.

22. Foucault,F., Vaury,C., Barakat,A., Thibout,D., Planchon,P., Jaulin,C., Praz,F. and Amor-Gueret,M. (1997) Characterization of a new BLM mutation associated with a topoisomerase II alpha defect in a patient with Bloom's syndrome. *Hum. Mol. Genet.*, **6**, 1427–1434.

23. Bernstein,D.A., Zittel,M.C. and Keck,J.L. (2003) High-resolution structure of the *E. coli* RecQ helicase catalytic core. *EMBO J.*, **22**, 4910–4921.

24. Ellis,N.A., Groden,J., Ye,T.Z., Straughen,J., Lennon,D.J., Ciocci,S., Proytcheva,M. and German,J. (1995) The Bloom's syndrome gene product is homologous to RecQ helicases. *Cell*, **83**, 655–666.

25. Liu,J.L., Rigolet,P., Dou,S.X., Wang,P.Y. and Xi,X.G. (2004) The zinc finger motif of *Escherichia coli* RecQ is implicated in both DNA binding and protein folding. *J. Biol. Chem.*, **279**, 42794–42802.

26. Hiratsuka,T. (1982) Biological activities and spectroscopic properties of chromophoric and fluorescent analogs of adenine nucleoside and nucleotides, 2′,3′-*O*-(2,4,6-trinitrocyclohexadienylidene) adenosine derivatives. *Biochim. Biophys. Acta*, **719**, 509–517.

27. Thompson,J.D., Higgins,D.G. and Gibson,T.J. (1994) CLUSTAL W: improving the sensitivity of progressive multiple sequence alignment through sequence weighting, position-specific gap penalties and weight matrix choice. *Nucleic Acids Res.*, **22**, 4673–4680.

28. Marti-Renom,M.A., Stuart,A.C., Fiser,A., Sanchez,R., Melo,F. and Sali,A. (2000) Comparative protein structure modeling of genes and genomes. *Annu. Rev. Biophys. Biomol. Struct.*, **29**, 291–325.

29. Gracy,J., Chiche,L. and Sallantin,J. (1993) Improved alignment of weakly homologous protein sequences using structural information. *Protein Eng.*, **6**, 821–829.

30. Luthy,R., Bowie,J.U. and Eisenberg,D. (1992) Assessment of protein models with three-dimensional profiles. *Nature*, **356**, 83–85.

31. Sippl,M.J. (1993) Recognition of errors in three-dimensional structures of proteins. *Proteins*, **17**, 355–362.

32. Vriend,G. (1990) WHAT IF: a molecular modeling and drug design program. *J. Mol. Graph.*, **8**, 52–5629.

33. Nicholls,A., Sharp,K.A. and Honig,B. (1991) Protein folding and association: insights from the interfacial and thermodynamic properties of hydrocarbons. *Proteins*, **11**, 281–296.

34. Janscak,P., Garcia,P.L., Hamburger,F., Makuta,Y., Shiraishi,K., Imai,Y., Ikeda,H. and Bickle,T.A. (2003) Characterization and mutational analysis of the RecQ core of the bloom syndrome protein. *J. Mol. Biol.*, **330**, 29–42.

35. Dou,S.X., Wang,P.Y., Xu,H.Q. and Xi,X.G. (2004) The DNA binding properties of the *Escherichia coli* RecQ helicase. *J. Biol. Chem.*, **279**, 6354–6363.

36. Hunt,J.B., Neece,S.H. and Ginsburg,A. (1985) The use of 4-(2-pyridylazo)resorcinol in studies of zinc release from *Escherichia coli* aspartate transcarbamoylase. *Anal. Biochem.*, **146**, 150–157.

37. Riddles,P.W., Blakeley,R.L. and Zerner,B. (1979) Ellman's reagent: 5,5′-dithiobis(2-nitrobenzoic acid)—a reexamination. *Anal. Biochem.*, **94**, 75–81.

38. Zhong,L. and Johnson,W.C.,Jr (1992) Environment affects amino acid preference for secondary structure. *Proc. Natl Acad. Sci. USA*, **89**, 4462–4465.

39. Xu,H.Q., Deprez,E., Zhang,A.H., Tauc,P., Ladjimi,M.M., Brochon,J.C., Auclair,C. and Xi,X.G. (2003) The *Escherichia coli* RecQ helicase functions as a monomer. *J. Biol. Chem.*, **278**, 34925–34933.

40. Tai,C.L., Pan,W.C., Liaw,S.H., Yang,U.C., Hwang,L.H. and Chen,D.S. (2001) Structure-based mutational analysis of the hepatitis C virus NS3 helicase. *J. Virol.*, **75**, 8289–8297.

41. Levin,M.K., Gurjar,M.M. and Patel,S.S. (2003) ATP binding modulates the nucleic acid affinity of hepatitis C virus helicase. *J. Biol. Chem.*, **278**, 23311–23316.

42. Xu,H.Q., Zhang,A.H., Auclair,C. and Xi,X.G. (2003) Simultaneously monitoring DNA binding and helicase-catalyzed DNA unwinding by fluorescence polarization. *Nucleic Acids Res.*, **31**, e70.

43. Luscombe,N.M., Austin,S.E., Berman,H.M. and Thornton,J.M. (2000) An overview of the structures of protein–DNA complexes. *Genome Biol.*, **1**REVIEWS001.

44. Mackay,J.P. and Crossley,M. (1998) Zinc fingers are sticking together. *Trends Biochem. Sci.*, **23**, 1–4.

45. Dawid,I.B., Breen,J.J. and Toyama,R. (1998) LIM domains: multiple roles as adapters and functional modifiers in protein interactions. *Trends Genet.*, **14**, 156–162.

46. Bahr,A., De Graeve,F., Kedinger,C. and Chatton,B. (1998) Point mutations causing Bloom's syndrome abolish ATPase and DNA helicase activities of the BLM protein. *Oncogene*, **17**, 2565–2571.

47. Neff,N.F., Ellis,N.A., Ye,T.Z., Noonan,J., Huang,K., Sanz,M. and Proytcheva,M. (1999) The DNA helicase activity of BLM is necessary for the correction of the genomic instability of Bloom syndrome cells. *Mol. Biol. Cell*, **10**, 665–676.

48. Banci,L., Bertini,I., Cramaro,F., Del Conte,R. and Viezzoli,M.S. (2003) Solution structure of Apo Cu,Zn superoxide dismutase: role of metal ions in protein folding. *Biochemistry*, **42**, 9543–9553.